Pergamon

0045-7949(94)00440-4

Computers & Structures Vol. 55, No. 2, pp. 265–268, 1995
Elsevier Science Ltd
Printed in Great Britain
0045-7949/95 $9.50 + 0.00

ENHANCED VISUALIZATION OF FAILURE MECHANISMS BY FINITE ELEMENTS

D. V. Griffiths† and **D. J. Kidger**‡

†Geomechanics Research Center, Colorado School of Mines, Golden, CO 80401, U.S.A.
‡Department of Engineering, University of Manchester, Manchester M13 9PL, U.K.

(*Received* 19 *September* 1993)

Abstract—The finite element method, in conjunction with elasto-plastic constitutive laws, is able to give accurate estimates of collapse loads in geotechnical problems. The mechanisms of failure produced by these analyses, however, are often diffuse and poorly defined, as compared with those assumed in classical limit analysis techniques. This paper describes two methods for improving their visualization. It is shown that by introducing a small degree of post-peak material softening into the constitutive law, a considerably more localized mechanism is achieved. In contrast to previous attempts to "trigger" mechanisms whereby select elements were weakened, all elements are given the same constitutive law in the present approach. A second method involves a re-gridding approach, together with the use of incremental displacements. In this approach, the displacement field is enhanced by interpolating between the nodal values.

INTRODUCTION

Although the finite element method can give good collapse load predictions (see e.g. [1, 2]), this is often achieved without reproducing in any detail the mechanisms assumed by the corresponding limit analyses. Conventional finite element meshes are constrained to remain continuous, so the deformed mesh at failure tends to indicate a rather diffuse failure mode. In any case, the greatest resolution that would ever be possible in a finite element mesh is governed by the size of the smallest elements in the failure zone.

A method used in the past to produce more localized failure mechanisms has been to introduce weak elements at strategic locations within the mesh [3]. This has the effect of "triggering" a mechanism which inevitably starts to form at the weakest point which has been artificially introduced. Of course, in reality, the strength profile of a material will be a *random* property with a mean and variance. This kind of material has been modelled by finite element analysis (see e.g. [4]) and leads to numerous shear bands triggered at the weakest elements. The "random field" approach to material modelling is certainly rational; however, this paper is concerned with improving the modelling of failure mechanisms in *homogeneous* materials.

This paper describes two methods of enhancing the failure mechanism within a finite element mesh in problems of slope stability. The first method uses a modification to the constitutive law incorporated in the material behaviour and represents a form of "triggering" but with the important difference that all elements are given the same properties throughout the mesh. The second method is purely interpretive and involves extracting as much information as possible from the finite element analysis by using the shape functions to interpolate the displacement field between the nodal values.

SLOPE STABILITY ANALYSIS

The field of slope stability represents a rather well-posed collapse problem in geomechanics for analysis by finite elements. One reason is that the problem is relatively unconfined, enabling a mechanism to form easily. Consequently, the flow rule is not of great importance in drained analyses, so a non-associated flow rule with no plastic volume change is usually sufficient to give adequate results.

The present work concentrates on "$\phi_u = 0$" soils, whose strength is suitably modelled by an elastic-perfectly plastic von Mises criterion. Figure 1 shows the finite element mesh of a slope resting on a foundation layer. The following properties were assigned to all elements of the mesh:

$$E = 1 \times 10^5 \text{ kPa}$$

$$\nu = 0.25$$

$$\gamma = 20 \text{ kN/m}^3$$

and the von Mises criterion in plane strain was defined as follows:

$$F = \bar{\sigma} - \sqrt{3} c_u, \qquad (1)$$

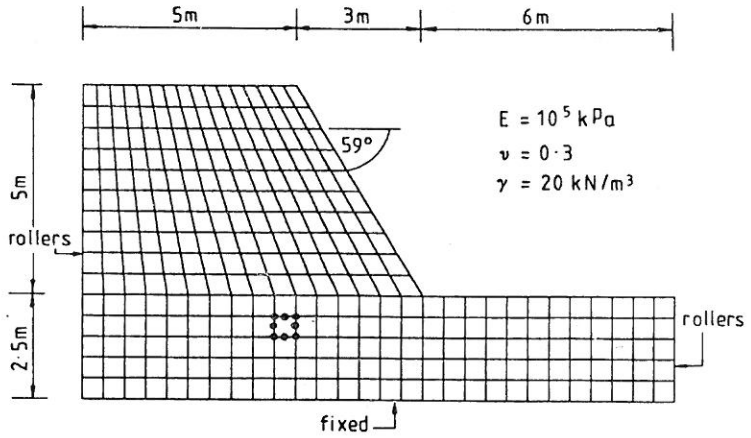

Fig. 1. Mesh used for softening analyses.

where

$$\bar{\sigma} = \frac{1}{\sqrt{2}}[(\sigma_x - \sigma_y)^2 + (\sigma_y - \sigma_z)^2 + (\sigma_z - \sigma_x)^2 + 6\tau_{xy}^2]^{1/2} \quad (2)$$

and c_u is the peak undrained shear strength of the soil.

The analysis proceeded by applying gravity loads to the slope with a fixed value of the shear strength c_u. If the slope remained stable, the analysis was repeated with a smaller value of c_u, and so on until failure occurred. Failure was deemed to have occurred when the algorithm hit an iteration count limit and the displacements increased rapidly. After each analysis, the maximum plastic displacement in the mesh was recorded, together with the number of iterations required to reach convergence. All analyses used a "viscoplastic" algorithm together with 8-node quadrilateral elements and reduced integration [5]. The results are presented in Fig. 2 as a graph of the maximum plastic displacement δ_{max} vs stability number N. The stability number is defined:

$$N = c_u/\gamma H,$$

where H = height of slope above foundation level; γ = total unit weight of soil.

The graph labelled ($M = 0$) corresponds to the perfectly plastic case and is seen to be in close agreement with Taylor's [6] solution ($N \approx 0.19$). Although the agreement with Taylor's limit analysis is very good, a rather diffuse failure mechanism is indicated by the deformed mesh shown in Fig. 3.

Introduction of softening

Greater localization of the failure mechanism can be achieved by introducing a small degree of post-peak softening into the constitutive law. This is a form of "triggering" but differs from other methods in that every element in the mesh is given the same softening property.

In order to define a "stress–strain" gradient, a strain invariant is introduced and defined as follows:

$$\bar{\epsilon} = \frac{\sqrt{2}}{3}[(\epsilon_x - \epsilon_y)^2 + (\epsilon_y - \epsilon_z)^2 + (\epsilon_z - \epsilon_x)^2 + \tfrac{3}{2}\gamma_{xy}^2]^{1/2}. \quad (3)$$

Under elastic plane strain conditions ($\epsilon_z = 0$),

$$\frac{\bar{\sigma}}{\bar{\epsilon}} = 3G, \quad (4)$$

where G is the elastic shear modulus.

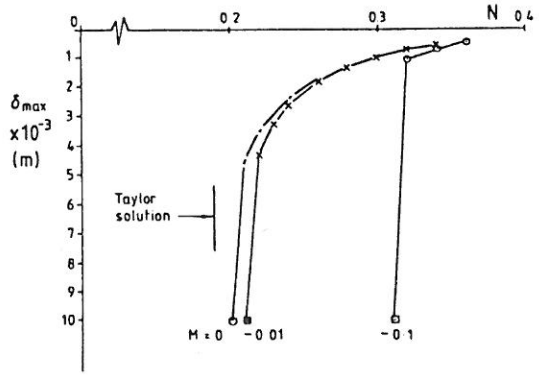

Fig. 2. Displacement vs stability number.

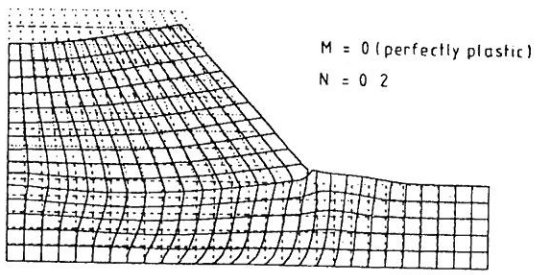

Fig. 3. Deformed mesh at failure ($M = 0$, perfectly plastic).

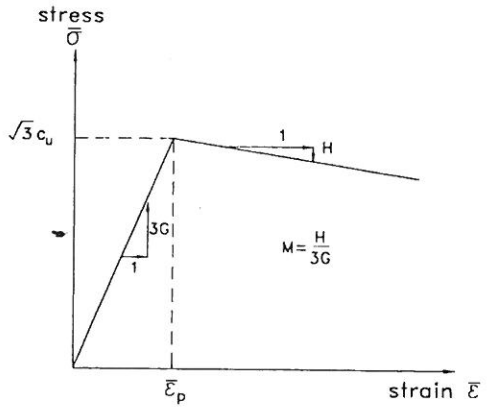

Fig. 4. Definition of softening parameter.

Once the peak strength is reached, the material starts to soften at a rate given by H, where

$$\frac{\bar{\sigma}}{\bar{\epsilon}} = H. \tag{5}$$

The degree of softening is measured by the dimensionless parameter M, which represents the ratio of the negative modulus of the material post-peak to its elastic value pre-peak, as shown in Fig. 4.

$$M = \frac{H}{3G}. \tag{6}$$

Perfect plasticity is obtained as a special case by letting $M = 0$.

Within the algorithm in which the peak strength is defined as c_p, the undrained shear strength c_u at any stage of the analysis and at any Gauss point is computed according to the following sequence:

$$c_u = c_p \qquad \text{if } \bar{\epsilon} \leqslant \bar{\epsilon}_p$$

$$c_u = c_p + H(\bar{\epsilon} - \bar{\epsilon}_p) \quad \text{if } \bar{\epsilon} > \bar{\epsilon}_p.$$

The analyses described previously were now repeated with a small degree of softening given by $M = -0.01$ (i.e. the softening gradient was just 1% of the pre-peak elastic value). Referring back to Fig. 2, it is clear that the softening has little effect on the computed stability number at failure (although the slightly increased value of N at failure is to be expected). The deformed mesh at failure, as shown in Fig. 5, is significantly different however. The softening has resulted in a much more localized mechanism, with certain elements experiencing virtually no plastic deformation and others being distorted significantly.

Further runs were performed with a greater degree of softening given by $M = -0.1$. As indicated in Fig. 6, this resulted in a further "sharpening" of the failure zone, but with the disadvantage that a significantly higher value of the stability number at failure was computed ($N \approx 0.31$). It appears that only a very small amount of softening can be allowed if the definition of the failure zone is to be improved *without* altering the collapse load to any great degree.

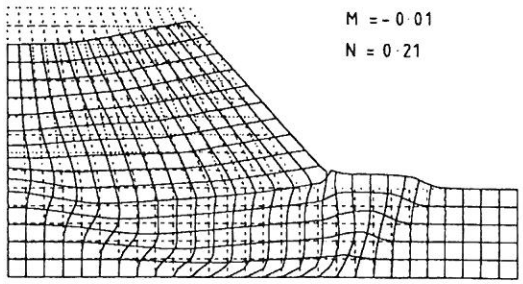

Fig. 5. Deformed mesh at failure ($M = -0.01$).

It can also be observed from Figs 5 and 6 that the degree of softening given by M influences the location of the failure zone. This is currently a topic of further investigation.

Re-gridding method

The previous method involved an alteration to the constitutive law in order to concentrate the shear strains in a more localized mechanism. Although it was shown that a very modest degree of softening was sufficient, the fact that the collapse load is altered by this modification is a disadvantage of the method.

Kidger [7] described an alternative approach in which a regular rectangular grid is superimposed on the finite element mesh. The location of each grid point is defined by the local coordinates of the parent element within which each is positioned. After the analysis has been performed and failure has been reached, the deformed grid is redrawn. This is achieved by retrieving the local coordinates of each grid point and plotting its position as defined by the new nodal coordinates. The grid plots are further enhanced by plotting the *difference* in displacements generated by two trial shear strength values just prior to failure.

Figures 7 and 8 show two meshes which were used to demonstrate the re-gridding technique. Both meshes have a slope angle of 26.6°, but with different foundation layer depths. The slopes were chosen to demonstrate two types of mechanism that would be predicted by Taylor's limit analysis approaches [6].

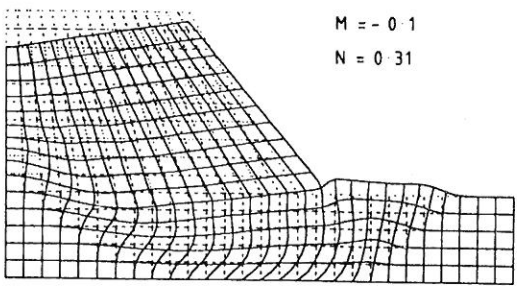

Fig. 6. Deformed mesh at failure ($M = -0.1$).

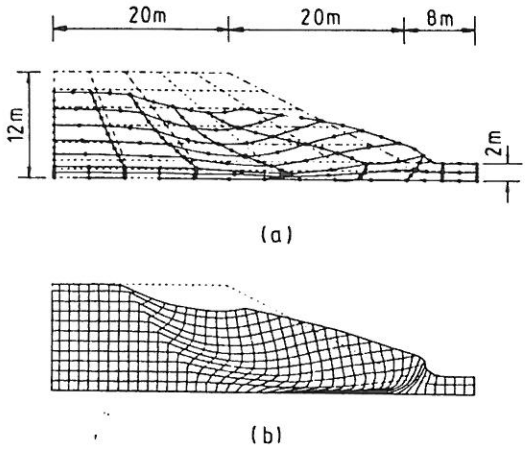

Fig. 7. Toe circle failure, (a) deformed mesh, (b) after re-gridding.

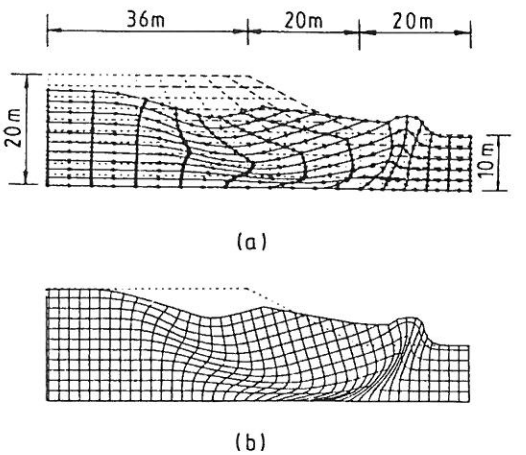

Fig. 8. Mid-point circle failure, (a) deformed mesh, (b) after re-gridding.

The first case failed at a stability number of $N \approx 0.14$ and Fig. 7(a) and (b) shows the deformed mesh and grid at failure respectively. The re-gridded plot [Fig. 7(b)] indicates a *toe circle* which is a tangent to the lower stratum and outcrops at the toe of the slope. The second case failed at a stability number of $N \approx 0.16$ and Fig. 8(a) and (b) shows the deformed mesh and grid at failure respectively. The re-gridded plot [Fig. 8(b)] indicates a *midpoint circle* which is a tangent to the lower stratum and whose centre lies on the centreline of the slope face. In all the plots, displacements were magnified for the sake of clarity. In both cases, the re-gridded plots gave a much clearer indication of the location of the failure mechanism than the plots of nodal displacements alone.

In each case, the finite element method gave stability numbers at failure that were in good agreement with classical limit solutions (see e.g. [8]).

CONCLUDING REMARKS

Two methods of enhancing the visualization of slope stability mechanisms have been described. Firstly, it was shown that by introducing a small degree of post-peak material softening into the constitutive law, a considerably more localized mechanism was achieved. All elements were given the same material properties, in contrast to previous attempts to "trigger" mechanisms whereby select elements were weakened. It was demonstrated, however, that if too much softening was incorporated, the failure load could be significantly altered.

A second approach involved re-gridding together with incremental displacements. This method assumed an elastic perfectly plastic material and gave well defined mechanisms without any need for "triggering" or alteration of the constitutive law. The method demonstrated that interpolation of the displacement field via the element shape functions leads to mechanism visualization, which would not be readily noticeable from the nodal displacements alone.

REFERENCES

1. O. C. Zienkiewicz, C. Humpheson and R. W. Lewis, Associated and non-associated viscoplasticity and plasticity in soil mechanics. *Géotechnique* **25**, 671–689 (1975).
2. D. V. Griffiths, Computation of bearing capacity factors using finite elements. *Géotechnique* **32**(3), 195–202 (1982).
3. J. H. Prevost, Localisation and deformation in elastic-plastic solids. *Int. J. Numer Anal. Meth. Geomech.* **8**, 187–196 (1984).
4. B. E. Hobbs and A. Ord, Numerical simulation of shear band formation in a frictional-dilational material. *Ing. Arch.* **59**, 209–221 (1989).
5. I. M. Smith and D. V. Griffiths, *Programming the Finite Element Method* (2nd Edn). John Wiley and Sons, Chichester (1988).
6. D. W. Taylor, Stability of earth slopes. *J. Boston Soc. Civ. Eng.* **24**, 197–246 (1937).
7. D. J. Kidger, Visualization of finite element eigenvalues and three dimensional plasticity. Ph.D. thesis, Department of Engineering, University of Manchester (1990).
8. K. Terzaghi and R. B. Peck, *Soil Mechanics in Engineering Practice*, p. 237. John Wiley and Sons, New York (1967).